One-dimensional elastic visco−plastic finite strain consolidation model for soft clay with uncertainty

by

Ding-Bao SONG, Ph.D., Postdoctoral fellow
Department of Civil and Environmental Engineering
The Hong Kong Polytechnic University, Hong Kong, China
Email: dingbao.song@polyu.edu.hk; Dingbao_song@126.com

Zhen-Yu YIN, Ph.D., Professor (corresponding author)
Department of Civil and Environmental Engineering
The Hong Kong Polytechnic University, Hong Kong, China
Email: zhenyu.yin@polyu.edu.hk

Peng-Lin LI, PhD student
Department of Civil and Environmental Engineering
The Hong Kong Polytechnic University, Hong Kong, China
Email: pengl.li@connect.polyu.hk

Jian-Hua YIN, Ph.D., Chair Professor
Department of Civil and Environmental Engineering
The Hong Kong Polytechnic University, Hong Kong, China
Email: jian-hua.yin@polyu.edu.hk

Abstract: Spatial variability of engineering properties caused by the natural characteristic heterogeneity is a common feature in soil layers. Meanwhile, changes in soil properties during consolidation and large strains are commonly encountered during long-term consolidation analysis of soft soils, however, few studies have considered these factors. A 1-D consolidation model fully coupled with elastic visco-plastic constitutive model, called EVPC, is developed using piecewise-linear method for long-term settlement of soft clay. The EVPC incorporates the idea of 'equivalent time' to account for large strain, soil self-weight, compressibility and permeability with spatial variability and high nonlinearity, as well as creep during the consolidation process. A comparison with finite element simulations and oedometer tests with different thicknesses of soil layer under multi-stage constant loads verified the effectiveness and accuracy of the EVPC's deterministic analysis. After that, the long-term settlement and excess pore pressure distribution of Berthierville clay layer from the field test are estimated using EVPC probabilistic analysis. All measurements from the field test are within the range of corresponded closely to the high probability density results of the probabilistic analysis, and the excess pore pressure is revealed to be more sensitive to the spatial variability of soil parameters than settlement.

Keywords: Soft soil; Consolidation; Finite strain; Viscoplasticity; Spatial variability; Uncertainty.

1 Introduction

As the demand for infrastructure has increased dramatically, many regions around the world have opted for extensive infrastructure constructions on reclaimed lands or thick soft soils. Foundation engineering is an indispensable aspect of such constructions; thus, the ability to accurately predict the settlement of soft soil foundations plays an important role in the construction, extending into facility maintenance and operation, especially for cases of assessing long-term consolidation behavior of foundations when a highly compressible soft clay layer is involved. Accurately predicting and calculating the long-term settlement of soft soil layers remains a challenge.

The cornerstone of settlement analysis is the consolidation theory. In specific terms, the one-dimensional consolidation theory pioneered by Terzaghi (1943), based on several assumptions, including constant compressibility and hydraulic conductivity, no creep occurs, ignore the soil self-weight and infinitesimal strain (i.e., small strain theory), has been adopted in practice because of its simplicity and clarity. However, it is usually not applicable for consolidation problems involving thick soft soils because of the inaccurate assessment of settlement caused by unrealistic assumptions (Xie and Leo, 2004).

Large strains are commonly encountered in practical projects involving the consolidation of preloaded soft soil layers. To overcome the limitation of small strain consolidation theory, McNabb (1960) presented a finite strain consolidation model with the void ratio as the privileged variable. Then, Gibson et al. (1967) proposed large-strain governing equations using Lagrangian coordinate system. Lee and Sills (1981) investigated the effect of soil self-weight on large strain consolidation based on the work of Gibson et al. (1967). McVay et al. (1989) improved Gibson's theory and

proposed an updated Lagrangian description of the governing equation to obtain an accurate variation of pore pressure during large strain consolidation process. Taking Gibson's theory as a departure point, Xie and Leo (2004) presented a fully explicit analytical solution for one-dimensional large-strain consolidation. Other researchers have made valuable contributions regarding consolidation modelling for soft soils under large strain conditions, including various solution techniques, such as finite element technique (Carter et al., 1979; Feldkamp, 1989), mathematical framework based on multiplicative plasticity (Borja and Alarcón, 1995; Borja et al., 1998; Zhao and Borja, 2020), piecewise-linear numerical models (Fox and Berles, 1997; Fox et al., 2003; Fox et al., 2014; Song et al., 2021), arbitrary Lagrangian-Eulerian (Nazem et al., 2008) and multi-constitutive neural network (Zhang et al., 2020). These models were developed based on the elastic or elastic-plastic compressibility constitutive relationships (i.e., stress-strain relationships are time-independent). On the other hand, a consensus has been achieved that soft soils exhibit inherent viscosity characteristics (i.e., time-dependent effects, including creep, strain rate dependency and relaxation), which are caused by the viscous physicochemical interactions that occur on a microscopic scale (Leroueil et al., 1985). Not taking creep effects into account in consolidation analysis may cause an inaccurate assessment of long-term settlement (Bjerrum, 1967; Garlanger; 1972). Even though software based on finite element method, such as PLAXIS, has been developed to account for large-strain consolidation problems, the issue of computational convergence remains a challenge, especially for the consolidation analysis of soil slurry under soil self-weight.

Bjerrum (1967) proposed an equivalent isochrone method to consider the time-dependent compressibility of soft soils by using a set of parallel "times lines", but unfortunately no

mathematical expressions were presented. Based on the isochrone concept, numerous elastic visco-plastic models have been developed (Garlanger, 1972; Vermeer and Neher, 1999; Yin et al., 2010). Yin and Graham (1989,1994) proposed an elastic visco-plastic (EVP) model with mathematical expression using equivalent timeline concept. Subsequently, this EVP model was incorporated into the one-dimensional consolidation equation in the context of infinitesimal strain theory to calculate the settlements and excess pore pressure of soil under multi-stage loads (Yin and Graham, 1996). Yin and Feng (2017) improved this work by presenting a simplified Hypothesis B method for EVP consolidation calculation with a more-explicit form. Combing with Gibson's theory, the EVP (Yin and Graham, 1989 and 1994) and the simplified Hypothesis B (Yin and Feng, 2017) were embedded in modelling the large-strain consolidation of soft soils with vertical drains (Hu et al., 2014; Nguyen et al., 2020). Based on the isotache concept, Xu et al., (2022) proposed a semi-analytical scheme for large-strain radial consolidation model that incorporates the soil destructuration and strain rate. The influence of soft soil consolidation under soil self-weight is neglected in these works. Li et al. (2023) improved the Yin-Graham EVP model by taking into account the soil self-weight, and then coupled this improved EVP into a finite strain consolidation model. Nevertheless, nonlinear creep and heterogeneity of soil layer are seldom considered in large-strain consolidation models.

Spatial variability in terms of physical and mechanical parameters caused by deposition and formation process, historical load conditions, and process of physical and chemical weathering (Yang et al., 2019), is another natural phenomenon in the soil layer. The soil parameters measured in the laboratory or on-site at a point location cannot accurately describe the engineering properties of the

entire soil layer. Consequently, it is essential to consider the spatial variability of soil parameters in the consolidation analysis. Presently, limited studies have applied random methods to study the fluid-solid fully coupled consolidation problems and are restricted to small-strain theory (Huang et al., 2010; Alibeikloo et al., 2022). Currently, probabilistic analysis of finite strain consolidation considering highly nonlinear and creeping soil parameters is still missing.

This paper aims to fill the aforementioned research gap regarding probabilistic analysis of elastic visco-plastic finite strain consolidation. A one-dimensional model, called EVPC, for elastic visco-plastic finite strain consolidation, is developed using piecewise-linear method in the current study. The EVP model presented by Yin and Graham (1989, 1994) was embedded in the EVPC model to consider the time-dependent compressibility relationships. EVPC takes into account the self-weight of soil, creep, large strain and variable coefficient of permeability in the procedure of consolidation. Additionally, EVPC includes time-dependent stress-strain constitutive relationships, time-dependent loading, secondary compression and spatial variability of nonlinear material properties. The development of EVPC model is presented, followed by verification by comparing the results of EVPC deterministic analysis to results from PLAXIS (soft soil creep model) and oedometer tests of specimens with different thicknesses. Lastly, EVPC probabilistic analysis to estimate the consolidation features of Berthierville clay in the field is presented.

2 Model description

2.1 Coordinate system

A saturated layer with an initial height of H_o is assumed as idealized two-phase material with incompressible pore water and solid particles; it is also assumed that only vertical strain would occur in the soil layer. The initial conditions (the time before the surcharged load Δq is applied) for the soil layer is illustrated in Fig. 1(a). The bottom of the soil layer is defined as the zero point of the longitudinal coordinate, z, and the positive direction of the longitudinal coordinate is the direction from bottom to up. Unlike other solution techniques, for the piecewise-linear method, the soil layer will be discretized by a certain number of elements prior to the consolidation calculation, as shown in Fig. 1(a). The soil layer is vertically subdivided into R_j elements, each of which had the same initial thickness of L_o. For each element, the vertical elevation z_j is determined by a node that located at the central of the element. At $t > 0$, as shown in Fig. 1(b), the height of the layer becomes H^t and the thickness of element j is denoted by L_j^t after a consolidation time t. The node of each element remained at the centre of its respective element in the procedure of consolidation, including the creep strain; additionally, the elevation of each node, z_j^t, is updated in each time step.

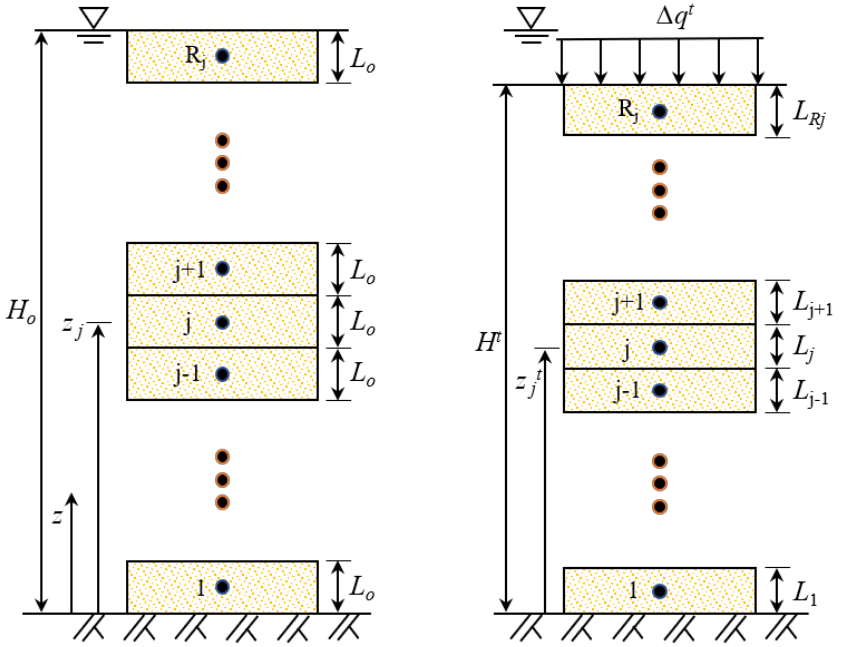

Fig. 1 Coordinate system for EVPC (a) initial conditions, and (b) conditions in the consolidation process

2.2 Random field of consolidation parameters

This study defined three natural soil properties, including plasticity index I_p, initial void ratio e_o, and liquid limit w_L, as random variables. The lognormal probability distribution is used to characterize the statistics of random variables to guarantee that the variable of interest would always be positive. The probability density function of random variables could be determined by mean value μ, standard deviation σ and autocorrelation length θ. Using the mean value and standard deviation, a dimensionless coefficient of variation COV can be obtained as follows:

$$COV_* = \frac{\sigma_*}{\mu_*} \tag{1}$$

where $*$ indicates the random variables (i.e., e_o, w_L or I_p).

Parameters for consolidation calculation, including compression index C_c, coefficient of permeability k, and secondary compression coefficient C_α, could be determined by equations with e_o, w_L and I_p, based on the evolutionary polynomial regression (EPR) methodology proposed by Jin et al. (2019, 2020), such as $C_c = f(e_o, w_L, I_p) + a_o$, where a_o is constant.

The variable interested $*$ is assumed to be lognormal distributed, which also implies that ln$*$ is normally distributed (Huang et al., 2010). σ_{ln*} and μ_{ln*} are given by

$$\sigma_{\ln^*} = \sqrt{\ln\left(1 + C_*^2\right)} \tag{2}$$

$$\mu_{\ln^*} = \ln \mu_* - 1/2\sigma_{\ln^*}^2 \tag{3}$$

where σ_{ln*} refers to the mean value of ln$*$; μ_{ln*} is the standard deviation of ln$*$.

Then, the desired lognormally distributed random field of variables is obtained according to σ_{ln*} and μ_{ln*}. Taking the random field of the initial void ratio as an example, this value could be expressed as

$$e_{o,j} = \exp\left(\mu_{\ln e_o} + \sigma_{\ln e_o} G_{\ln e_o, j}\right) \tag{4}$$

where $e_{o,j}$ is the initial void ratio for element j, $G_{\ln e_o, j}$, related to the autocorrelation length $\theta_{\ln^*}$ is a normally distributed random field with zero mean value and unit variance and is generated by the Cholesky Decomposition (CD) technique with an exponential autocorrelation function. The single exponential (SNX) autocorrelation function, which has been widely adopted in probabilistic analysis because of its computational simplicity (Griffiths and Fenton, 2004; Salgado and Kim, 2014), is expressed as follows:

$$\rho_{\ln^*}\left(z_{i,j}\right) = \exp\left(\frac{-2|\Delta z|}{\theta_{\ln^*}}\right) \tag{5}$$

where ρ represents the autocorrelation coefficient between two random variable values at any two points, e.g., z_i and z_j, and $\Delta z = z_i - z_j$. In the EVPC model, z_i and z_j are the node positions of elements i and j, respectively. Moreover, the correlations between different variables needed to be considered when there are multiple random variables. The cross-correlations between e_o, w_L and I_p (i.e., ρ_{e_o,w_L}, ρ_{e_o,I_p} and ρ_{w_L,I_p}) are also considered.

2.3 Constitutive relationships

For the elastic and elastoplastic compressibility models, the relationships of void ratio e (or vertical strain) and effective stress σ' have a one-to-one correspondence for a certain soil layer. Any variation in the void ratio is only caused by a corresponding change in effective stress, and their relationship is independent of time, which differed from the EVP model. The elastic visco-plastic constitutive proposed by Yin and Graham (1996) using the idea of 'equivalent time' was fully incorporated into the EVPC. In that model, the compression under the surcharge loading consists of three components: (a) instantaneous strain, ε^e, (b) stress-dependent plastic strain, ε^r, and (3) creep strain, ε^{tp}.

$$\varepsilon^e = \varepsilon_i^e + \kappa / V \times \ln\left(\sigma' / \sigma_i'\right) \tag{6-1}$$

$$\varepsilon^r = \varepsilon_o^r + \lambda / V \times \ln\left(\sigma' / \sigma_{ro}'\right) \tag{6-2}$$

$$\varepsilon^{tp} = \psi / V \times \ln\left[\left(t_o + t_e\right) / t_o\right] \qquad -t_o \prec t_e \prec \infty \tag{6-3}$$

where κ, λ and ψ refer to soil parameters for instantaneous strain, stress-dependent plastic strain and creep strain, respectively, σ_i' indicates a unit of effective stress, ε_i^e is the strain at $\sigma' = \sigma_i'$, the parameter σ_{ro}' is similar to pre-consolidation pressure, ε_o^r signifies the strain at $\sigma' = \sigma_{ro}'$ and is

193 related to initial void ratio e_o, t_o signifies the parameter for selecting the reference timeline, and t_e is
194 the equivalent time. Lastly, V denotes the specific volume, which is equal to 1+e. Furthermore, it
195 should be noted that the instantaneous strain is elastic, time-independent and reversible.

196 Once the t_e is determined, the relationships of stress and strain at any state (σ', ε) could be
197 expressed as

198 $$\varepsilon = \varepsilon^r + \varepsilon^{vp} = \varepsilon_o^r + \lambda / V \ln\left(\sigma' / \sigma'_{ro}\right) + \psi / V \ln\left[\left(t_o + t_e\right) / t_o\right] \tag{7}$$

199 and could be rewritten in the form of $e - \sigma'$, as follows:

200 $$e = e_o^r - \lambda \ln\left(\sigma' / \sigma'_{ro}\right) - \psi \ln\left[\left(t_o + t_e\right) / t_o\right] \tag{8}$$

201 If the stress-strain state is not on the 'equivalent time line', t_e is determined as

202 $$t_e = -t_o + t_o \exp\left[\left(e_o^r - e\right) / \psi\right]\left(\sigma' / \sigma'_{ro}\right)^{-\lambda/\psi} \tag{9}$$

203 where the term '$\exp\left[\left(e_o^r - e\right) / \psi\right]\left(\sigma' / \sigma'_{ro}\right)^{-\lambda/\psi}$' is equivalent to '$\left[\psi / (1 + e_0^r)\right]\left(\sigma' / \sigma'_{ro}\right)^{(\lambda-\kappa)/\psi}$' in the
204 creep-based models of Kutter and Sathialingam (1992) and Vermeer and Neher (1999) and the
205 rate-dependency-based models proposed by Yin et al. (2010, 2011).

206 After applying an increment load $\Delta\sigma'$ for a duration time Δt, the decrease void ratio Δe is the
207 sum of an elastic void ratio decrement Δe^e and a visco-plastic void ratio decrement Δe^{vp}; among them,
208 Δe^{vp} is composed of stress-dependent plastic and creep compressions (i.e., Δe^r and Δe^c), as shown in
209 Fig. 2(a).

210 $$\Delta e = \Delta e^e + \Delta e^{vp} \tag{10}$$

211 which could also be expressed as

212 $$\Delta e = \frac{\kappa}{\sigma'} \Delta\sigma' + \frac{\Delta e^{vp}}{\Delta t} \Delta t \tag{11}$$

213 and then the variation rate of void ratio $\dot{e}$ is

$$\dot{e} = \dot{e}^{e} + \dot{e}^{vp} = \frac{\Delta e}{\Delta t_e} = \frac{\Delta e^{e}}{\Delta t_e} + \frac{\Delta e^{vp}}{\Delta t_e} \tag{12}$$

Since the elastic compression is time-independent, $\Delta e^{e} / \Delta t_e = 0$, combining Eq. 9 and Eq. 12 give

$$\frac{\Delta e}{\Delta t_e} = \frac{\Delta e^{vp}}{\Delta t_e} = \frac{\psi}{t_o + t_e} = \frac{\psi}{t_o} \exp\left(\frac{e - e_o^{r}}{\psi}\right)\left(\frac{\sigma'}{\sigma'_{ro}}\right)^{\lambda/\psi} = \frac{\Delta e^{vp}}{\Delta t} \tag{13}$$

Next, the relationship of Δe - $\Delta \sigma'$ - Δt is determined as

$$\Delta e = \frac{\kappa}{\sigma'} \Delta \sigma' + \frac{\psi}{t_o} \exp\left(\frac{e - e_o^{r}}{\psi}\right)\left(\frac{\sigma'}{\sigma'_{ro}}\right)^{\lambda/\psi} \Delta t \tag{14}$$

where κ, λ, ψ, σ'_{ro}, e_o^{r} and t_o represent six parameters used in the elastic visco-plastic model (Yin and Graham, 1996). If Δe and Δt are known, the variation of effective stress for time increment Δt is computed as follow

$$\Delta \sigma' = \left(\Delta e - \frac{\psi}{t_o} \exp\left(\frac{e - e_o^{r}}{\psi}\right)\left(\frac{\sigma'}{\sigma'_{ro}}\right)^{\lambda/\psi} \Delta t \right) \times \frac{\sigma'}{\kappa} \tag{15}$$

Fig. 2(b) shows the hydraulic conductivity constitutive relationship for EVPC, which is defined by *Rn* pairs of $\overline{e} - \overline{k}$. Any required form of hydraulic conductivity relationship can be represented in this method. Besides, specific mathematical expressions of the hydraulic conductivity constitutive relationship can also be adopted in the EVPC model.

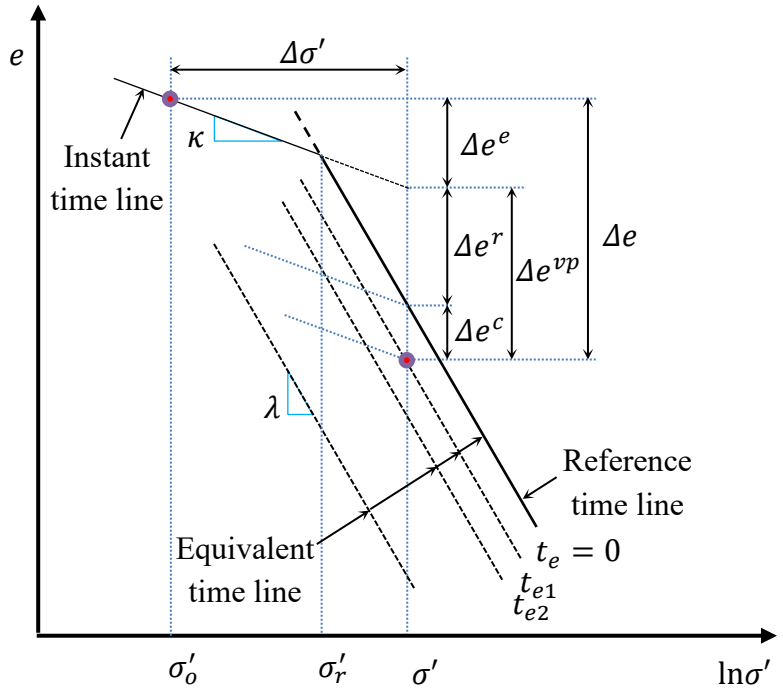

(a)

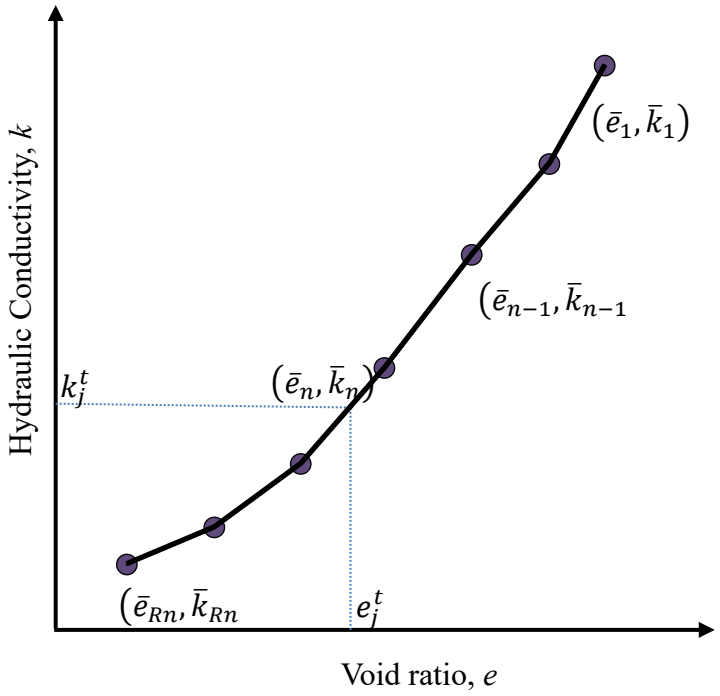

(b)

Fig. 2 Illustration of constitutive relationship for: (a) elastic visco-plastic compressibility, and (b) hydraulic conductivity

2.4 Stress, flow, boundary conditions and settlement

The total vertical stress σ is composed of the effective stress at initial condition q_o, surcharge load Δq and self-weight of soil. In the consolidation procedure, the total vertical stress for element j, σ'_j is determined by

$$\sigma_j^t = \left(H_w - H^t\right)\gamma_w + \frac{L_j^t \gamma_j^t}{2} + \sum_{b=j+1}^{R_j} L_b^t \gamma_b^t + q_o + \Delta q \tag{16}$$

where H_w represents the water table height, γ_w is the unit weight of pore water, $\gamma_j^t = \left(G_s + e_j^t\right)/\left(1 + e_j^t\right)\gamma_w$ denotes the saturated unit weight, G_s refers the specific gravity of solids and e_j^t indicates the void ratio in the consolidation procedure.

Once the effective stress is known, the pore water pressure u and excess pore water pressure u_e could be determined on the basis of effective stress principle.

$$u_j^t = \sigma_j^t - \sigma_j'^t \tag{17}$$

$$u_{e,j}^t = u_j^t - \left(H_o - z_j^t\right)\gamma_w \tag{18}$$

The equivalent series hydraulic conductivity and hydraulic gradient at time t for adjacent element nodes j and j-1 (i.e., $k_{s,j}^t$ and i_j^t) are calculated as

$$k_{s,j}^t = \frac{k_{j+1}^t k_j^t \left(L_{j+1}^t + L_j^t\right)}{L_{j+1}^t k_j^t + L_j^t k_{j+1}^t} \tag{19}$$

$$i_j^t = \frac{h_{j+1}^t - h_j^t}{z_{j+1}^t - z_j^t} \tag{20}$$

where k_j^t denotes the coefficient of permeability, and $h_j^t = z_j^t + u_j^t / \gamma_w$ calculates the total head for element j at consolidation time t.

Once the equivalent series coefficient of permeability and hydraulic gradient are determined, the flow rate out of (into) element adjacent elements j and j-1 at consolidation time t, $v_{rf,j}^{t}$ could be calculated as follow

$$v_{rf,j}^{t} = -k_{s,j}^{t} i_{j}^{t} \tag{21}$$

The top and bottom boundaries could be specified as impermeable or free drainage, respectively, as illustrated in the following equations:

$$i_{Rj} = \frac{H_w - h_{R_j}^{t}}{H^{t} - z_{R_j}^{t}} \quad \text{top boundary (drained)} \tag{22a}$$

$$i_{Rj} = 0 \quad \text{top boundary (undrained)} \tag{22b}$$

$$i_o = \frac{h_1^{t} - H_w}{z_1^{t}} \quad \text{bottom boundary (drained)} \tag{22c}$$

$$i_o = 0 \quad \text{bottom boundary (undrained)} \tag{22d}$$

Then, the height of element j after the time increment Δt is determined to be

$$L_j^{t+\Delta t} = L_j^{t} - (v_{rf,j}^{t} - v_{rf,j-1}^{t})\Delta t \tag{23}$$

and the void ratio could be updated as

$$e_j^{t+\Delta t} = \frac{L_j^{t+\Delta t}(1+e_{o,j})}{L_o} - 1 \tag{24}$$

The void ratio decrement for the increment time Δt, $\Delta e_j^{\Delta t}$, is calculated as the difference of the void ratio for the time increment Δt

$$\Delta e_j^{\Delta t} = e_j^{t} - e_j^{t+\Delta t} \tag{25}$$

Using the $\Delta e_j^{\Delta t}$, the increment of effective stress for the time increment $\left(\Delta\sigma'\right)^{\Delta t}$ is computed using Eq. (15).

At consolidation time $t + \Delta t$, the thickness and settlement of the layer (i.e., $H^{t+\Delta t}$ and $S^{t+\Delta t}$) are, respectively,

$$H^{t+\Delta t} = \sum_{j=1}^{R_j} L_j^{t+\Delta t} \tag{26}$$

$$S^{t+\Delta t} = H_o - H^{t+\Delta t} \tag{27}$$

2.5 EVPC flow chart

Fig. 3 illustrates the basic principle of the calculation loop of EVPC model. EVPC has two different calculation functions: deterministic analysis and probabilistic analysis, the latter considering the spatial variability of compression and permeability parameters. For the deterministic analysis, input data, which included the initial height H_o, element number R_j, initial void ratio e_o, initial effective stress σ'_o, applied surcharge loads Δq, specific gravity of solids G_s (G_s = 1 when the self-weight is ignored), parameters for elastic visco-plastic constitutive model (i.e., κ, λ, ψ, σ'_{ro} and t_o), hydraulic conductivity, the boundary drainage conditions and the termination calculation time, are directly assigned a definite value or equation to begin the calculation. For probabilistic analysis, the consolidation calculation model is embedded in a Monte Carlo framework. Then N_f groups of R_j random values are generated for each random variable, and the random values of each group of random variables are assigned to the corresponding elements in each Monte Carlo simulation, where N_f refers to the maximum times for Monte Carlo simulations. The initial thickness for each element and initial elevation for each node are computed before the main compute loop. For the first main iterative procedure, the excess pore water pressure for each element is computed from q_o (Eq. 16 and Eq. 17).

Next, the hydraulic conductivity is determined for all of the elements based on the relationships of *e-k*, followed by combining the total head of each element to calculate the relative discharge velocity of adjacent nodes during increment time Δt. Element thickness and void ratio for each element are updated, as well as the void ratio decrement, soil layer height and settlement. The calculation sequence of the main loop is repeated with Δe_j, L_j and H until the user-specified consolidation calculation time t_f is reached. The above consolidation calculation loop is repeated until N_f groups of Monte Carlo simulations are completed.

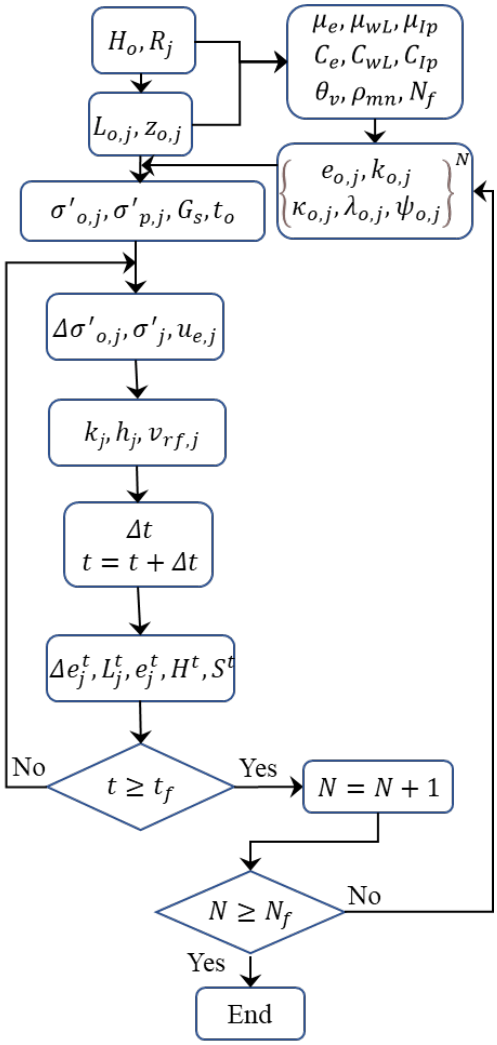

Fig. 3 Flow chart for the EVPC model

3 Model validation with deterministic analysis

The accuracy and capacities of the deterministic analysis of EVPC model are verified by comparing the calculations from EVPC with solutions from the FEM software PLAXIS and measurements from oedometer tests.

3.1 Comparison with PLAXIS

The accuracy and performance of EVPC are first determined by comparing the results from the EVPC with those from the finite element software PLAXIS. Four soil layers with different initial heights H_o (1, 2, 5 and 10 m) are used for this verification problem. In addition, the soft soil creep model (i.e., SSC model) is used in the PLAXIS simulation, and updated mesh and updated water pressure analysis are adopted in PLAXIS simulations to take into account the finite strain. The detailed parameters used in the simulations are listed in Table 1, in which C_k refers to the change index of hydraulic conductivity and is defined as the relationships of e-log$k$ (meaning $k = k_o \times 10^{(e-e_o)/C_k}$, and the only availabe k-e relationship in PLAXIS), and k_o is the coefficient of permeability corresponding to e_o. Note that EVPC essentially accounts for any desired k-e form. An instantaneous stress increment Δq = 20 kPa was applied and thereafter was held constant.

Table 1. Soil parameters for PLAXIS and EVPC simulations

κ	λ	ψ	e_o	$\sigma_o^{'}$ (kPa)	$\sigma_p^{'}$ (kPa)	C_k	k_o (m/min)	t_o (min)
0.025	0.25	0.0125	1.5	1	10	0.8	1.0×10^{-6}	1440

The comparative plots of settlement versus log t for different heights of soil layers are displayed in Fig. 4. The EVPC settlement simulation and PLAXIS results can be seen to demonstrate exact

agreement. The settlements at 10^5 days for H_o = 1 m, 2 m, 5 m and 10 m are 0.13 m, 0.26 m, 0.66 m and 1.31 m, respectively, corresponding to a strain of about 13%.

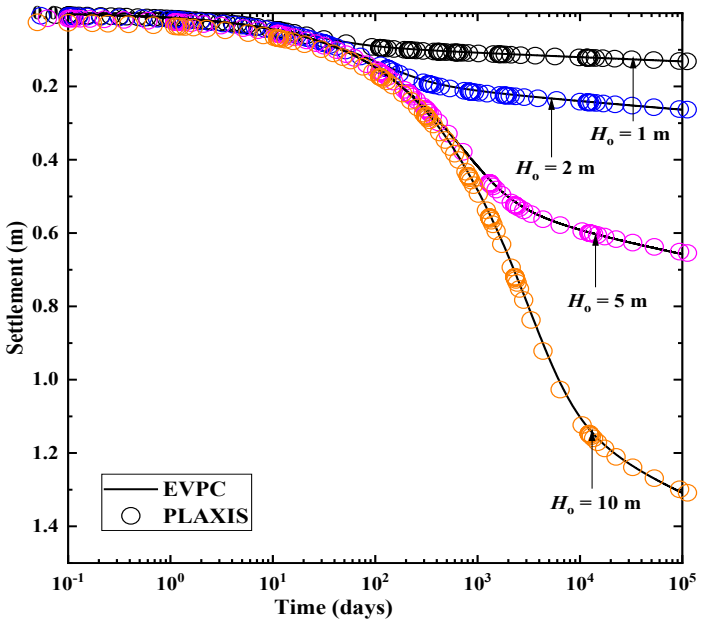

Fig. 4 Comparison of EVPC and PLAXIS for settlement of various heights of soil layers

Another case involved step loads. Here, Δq = 20, 40 and 60 kPa are applied at t = 0, 10 and 100 days, respectively. A soil layer of H_o = 1.0 m with the same soil parameters given in Table 1 was used for simulation verification. Fig. 5 compares the settlement results from simulations of EVPC and PLAXIS. At 10^5 days, the settlement is about 0.24 m, indicating a strain of 24%, which corresponded to a large-strain consolidation problem. Settlement results for the middle and late consolidation stages of PLAXIS are slightly smaller than those of EVPC. This is maybe partly because the updated water pressures procedure results in a smaller effective surcharge load that applied on the soil, and partly because the calculation error between different numerical approaches, especially for large strain and complex loading conditions. Fig. 6 compares the excess pore water pressure versus log$t$ from the simulations of EVPC and PLAXIS. The initial excess pore water pressure from PLAXIS is

334 slightly smaller than that from EVPC, corresponding to the smaller settlement in the middle and late

335 consolidation stages of PLAXIS. Generally, all of the plots agreed satisfactorily.

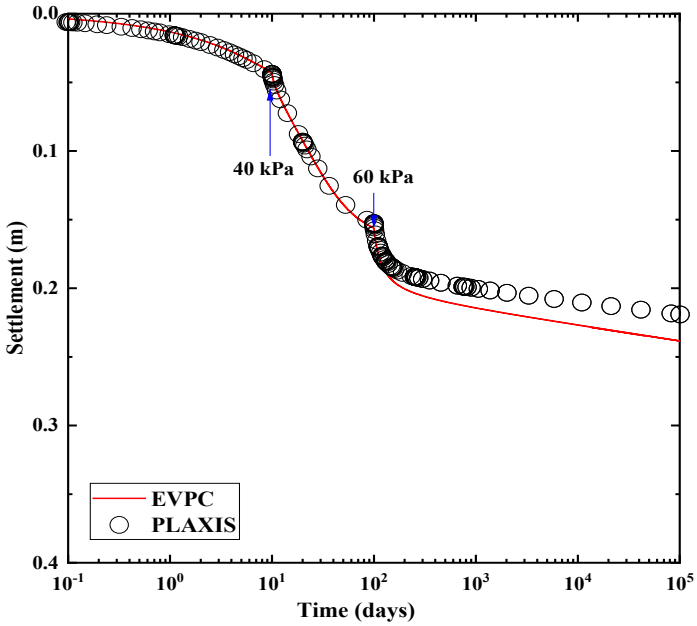

336

337 Fig. 5 Comparison of EVPC and PLAXIS for settlement of step loading

338

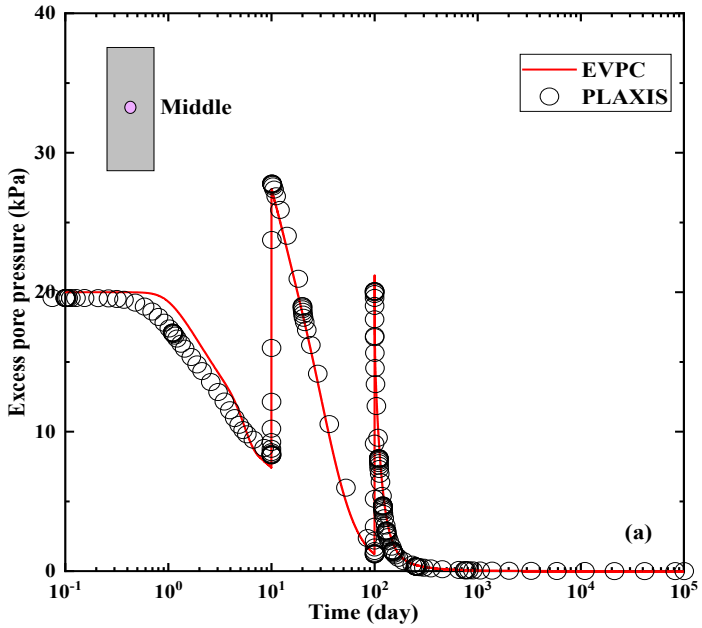

339

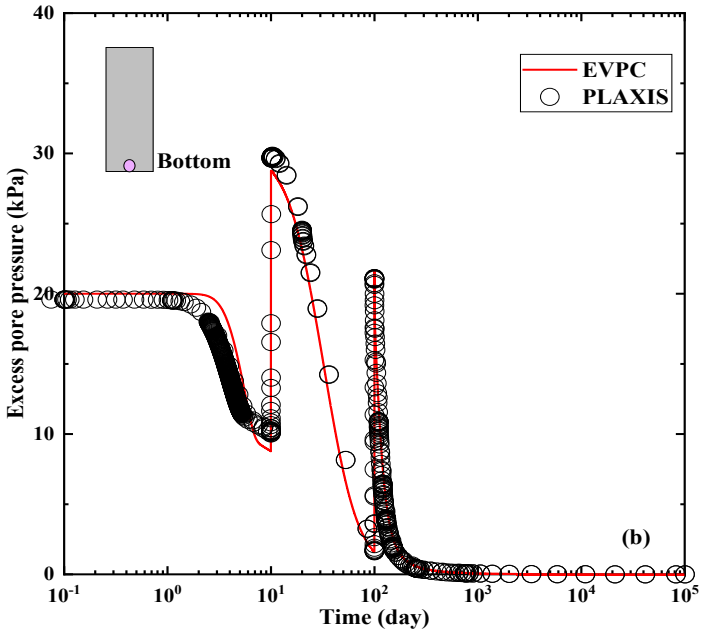

Fig. 6 Comparison of EVPC and PLAXIS simulations for u_e in: (a) middle and (b) bottom

3.2 Comparison with oedometer tests

Modified oedometer tests on the varying height of marine clay were conducted by Berre and Iversen (1972), including four different initial thicknesses: 0.0188 m (test 7), 0.0757 m (test 6), 0.15 m (test H6) and 0.45 m (test H4). The settlement and excess pore pressure (at the bottom of specimen) were measured during testing. The specimen for test H4 combined three segments, with each segment 15 cm in height. The top and bottom boundaries of the specimens were set as permeable and impermeable, respectively, and free drainage was set at the top boundary of the first segment for test H4.

The clay used for the oedometer tests was taken from Drammen, Norway, with a diameter $\phi =$ 95 mm sample at a depth of 5.2-6.7 m. The natural water content and Atterberg limits of the Drammen clay are 57-60%, 54-60% (liquid limit) and 28-34% (plastic limit), respectively, and the content of particles less than 2 μm is 45%, as provided by Berre and Iversen (1972).

Five-stage loading with various time durations was included in the oedometer tests, and two of five stages (increments 4 and 5) are selected for simulations with the detailed data presented in Table 2. H_o represents the initial height of specimen, while ε_o is the cumulative strain caused by previous load increments. Note that increment 4 covering the situ stress and increment 5 above the situ stress, indicating that the specimens were slightly over-consolidated in increment 4 and were normally consolidated in increment 5. The excess pore water pressure of specimens, $u_e = 0$ for the end of the load increment, indicating that the effective stress of specimens is at equilibrium and is equal to the previous total load stress.

Table 2. Oedometer test parameters (after Berre and Iversen, 1972)

Test	H_o (m)	Increment	ε_o (%)	σ_o' (kPa)	σ_{ro}' (kPa)	Δq (kPa)	t (min)
7	0.0188	4	2.25	55.3	92.5	37.2	7055
		5	6.08	92.5	140.2	47.7	10000
6	0.0757	4	1.25	55.9	93.3	37.4	8060
		5	5.51	93.9	140.5	46.7	5694
H6	0.15	4	1.20	55.2	92.5	37.3	11230
		5	4.53	92.5	140.2	47.7	10000
H4	0.45	4-Top	1.15	53.4	89.2	35.8	30440
		4-Middle	1.25	53.4	89.2	35.8	30440
		4-Bottom	1.50	53.4	89.2	35.8	30440
H4	0.45	5-Top	4.25	89.2	134.7	45.5	61450
		5-Middle	5.21	89.2	134.7	45.5	61450
		5-Bottom	6.30	89.2	134.7	45.5	61450

Table 3. Parameters for simulation of oedometer tests (based on test 7 after Berre and Iversen, 1972)

κ	λ	ψ	e_o	σ_r' (kPa)	C_k	k_o (m/min)	t_o (min)
0.0092	0.3634	0.0081	1.30	79.2	0.0965	6.2×10^{-8}	1440

The soil parameters used for the EVPC simulations, as presented in Table 3, are derived from the measured data from test 7. Fig. 7 compares the EVPC calculations and the measurements from test 7, including plots of average strain versus log t (Fig. 7a) and excess pore water pressure (Fig. 7b) versus log t for increments 4 and 5. Since the parameters of Drammen clay applied to the EVPC are determined from the data of test 7, it can be expected that the outcomes will show a good consistency, especially for the comparison of settlement strain. The u_e calculated by the EVPC agreed well with the measured data for measured time $t \geq 1$ min. Using the same soil parameters, the consolidation behaviour of the specimens in tests 6, H6 and H4 are predicted by the EVPC.

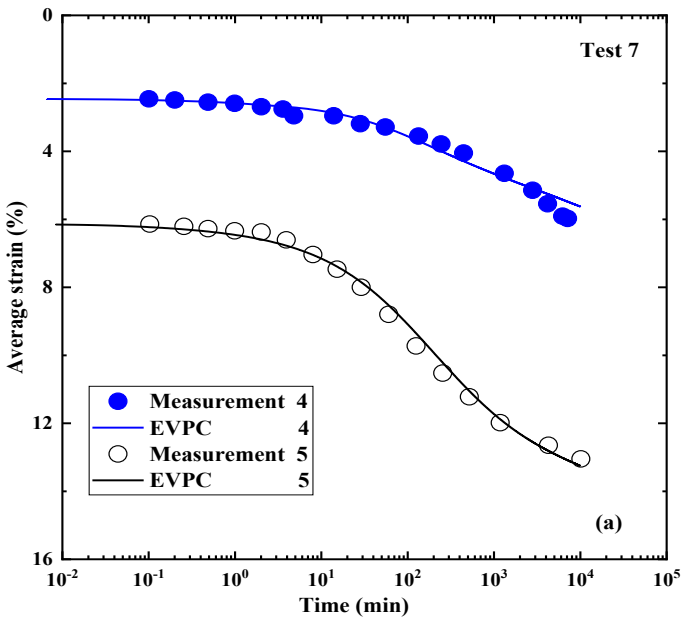

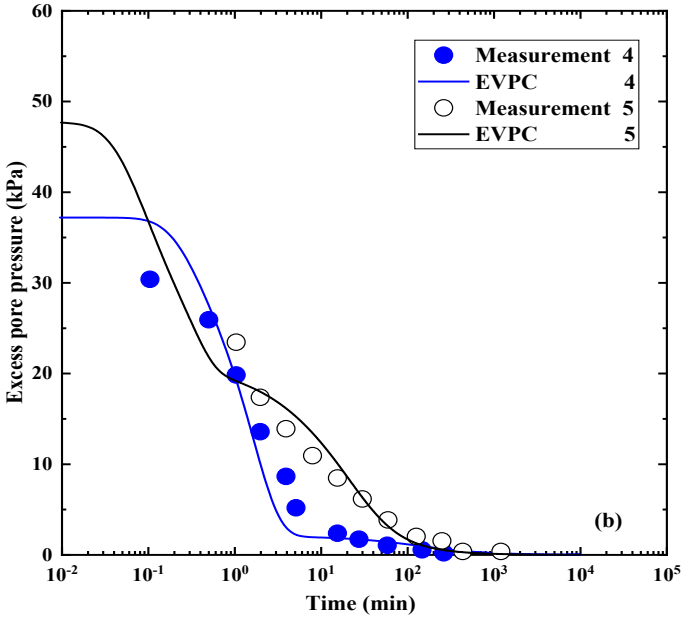

Fig. 7 Comparison of EVPC simulation and measurements from test 7: (a) average strain vs log t and (b) u_e vs log t

Figs. 8(a) and 8(b) illustrate the comparative plots of average strain versus log t and u_e versus log t, respectively, for increments 4 and 5 of test 6. The prediction results for average strain by the EVPC corresponded closely to the measured values. The measured initial excess pore water pressure is lower than outcomes from EVPC simulations and the expected values based on increment loads (i.e., 37.4 kPa for increment 4 and 47.7 kPa for increments 5), especially in the case of increment 4.

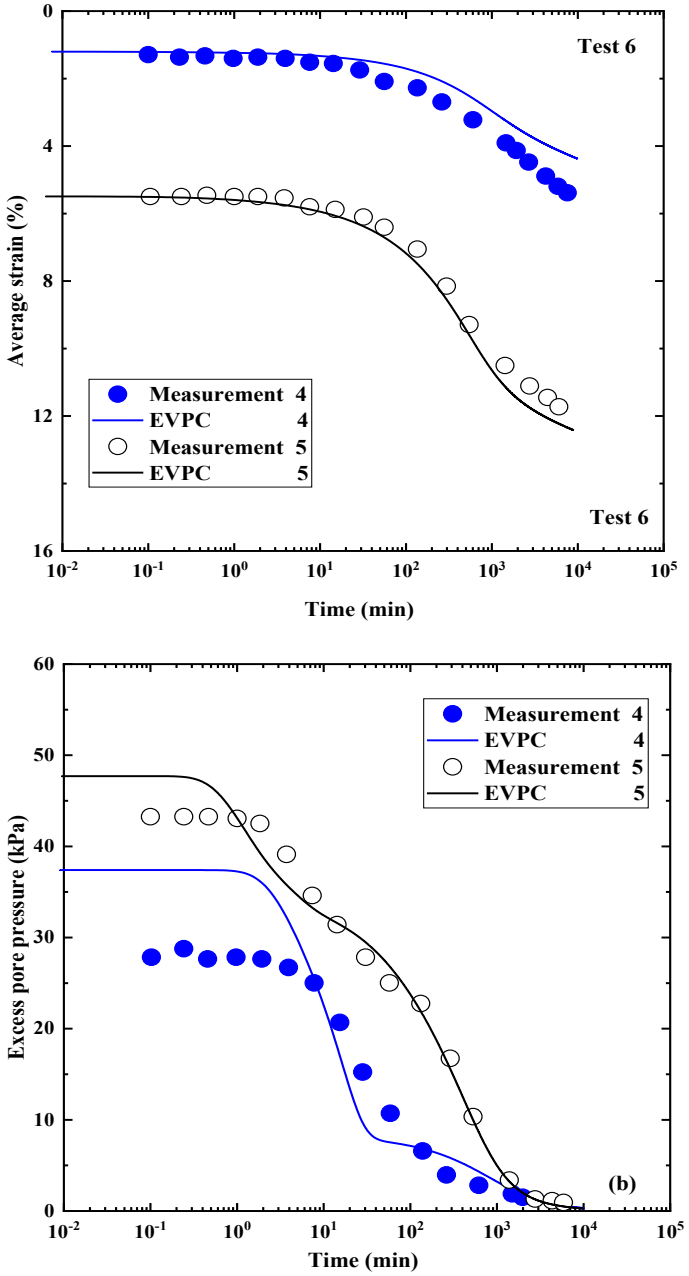

386

387

388 Fig. 8 Comparison of EVPC simulation and measurements from test 6: (a) average strain vs log t and

389 (b) u_e vs log t

390

391 The comparison of results of average strain from EVPC simulation and measurements from test

392 H6, as shown in Fig. 9(a), reveal satisfactory agreement. The predicted u_e at early stage of

393 consolidation (within 10 mins after the application of incremental loads) is larger than the measured

394 value (Fig. 9b); however, they agreed more closely when the test elapsed time is longer than 10 mins.

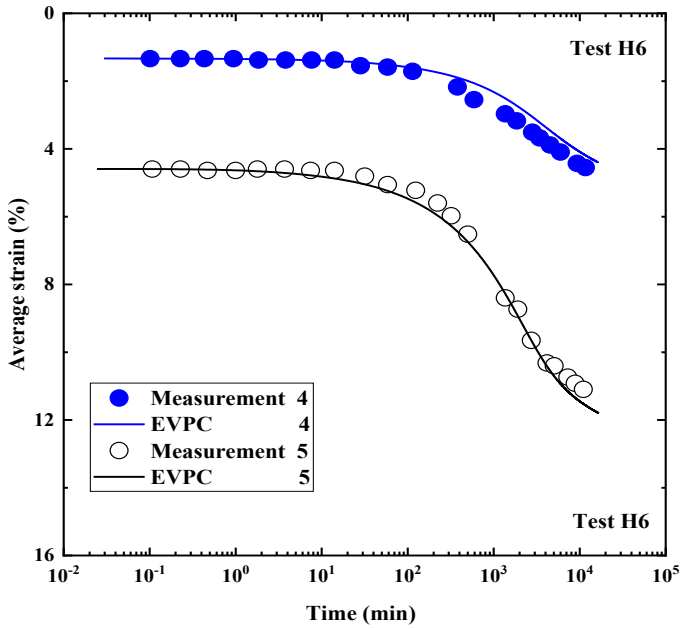

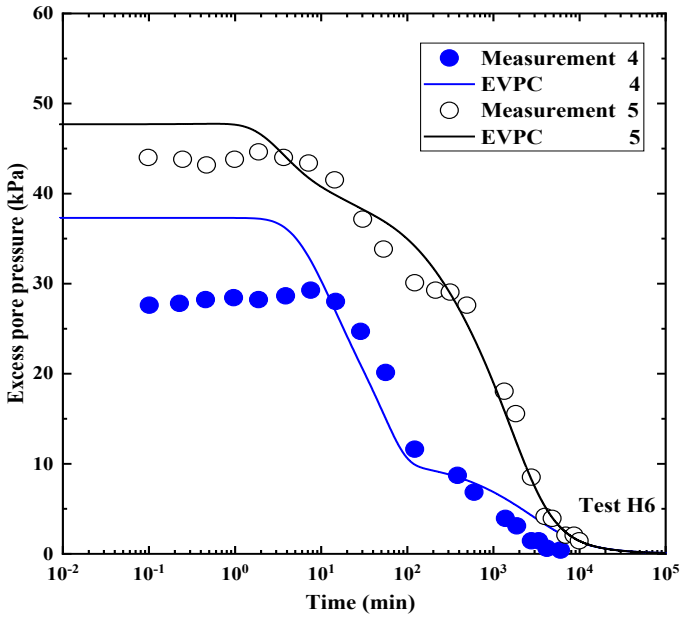

Fig. 9 Comparison of EVPC simulation and measurements from test H6: (a) average strain vs log t and (b) u_e vs log t

The average strains calculated by the EVPC are consistent with the measured data from test H4 (Fig. 10a). Once again, the measured excess pore water pressure at early stage of consolidation (within about 100 mins after the application of incremental loads) is lower than the estimated results, especially for increment 4. The calculation results underestimated the excess water pressure in the

middle stage of consolidation testing as presented in Fig. 10(b). In comparison with increment 4, the prediction results of u_e for increment 5 corresponded closely to the monitoring data, as illustrated in Fig. 10(c), and the predicted values slightly overestimated the u_e. Furthermore, the measured data uncovered that the u_e near the bottom of the lower specimen (i.e., impervious boundary) increased slightly after the load increment, a phenomenon that the EVPC is also able to simulate (Fig. 10c). An excess pore pressure slightly higher than the applied load near the bottom boundary during the early consolidation stage is observed in the increment 5 test H4 both for oedometer test and EVPC simulation. This phenomenon results from the relaxation of the section in the soil prior to the discharge of pore water. In the case of relaxation with constant volume and constant total stress, the reduction of effective stress must be balanced by an increase in excess pore pressure, which is consistent with the findings of Yin et al. (1994).

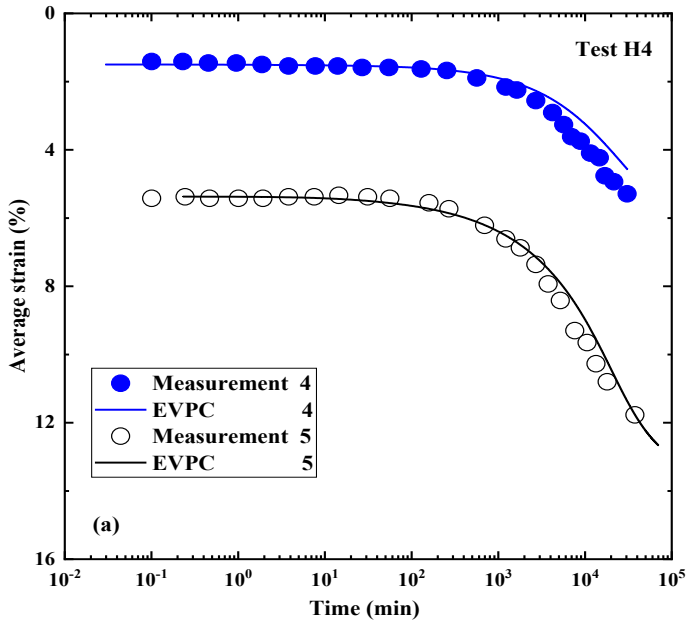

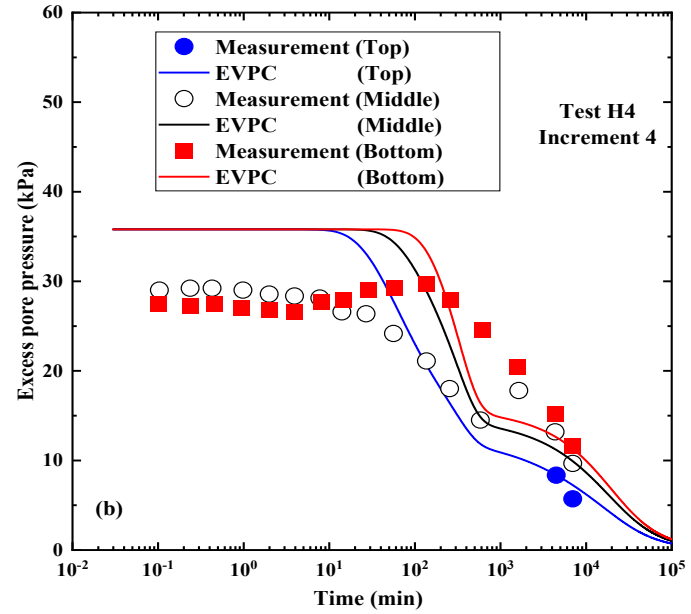

416

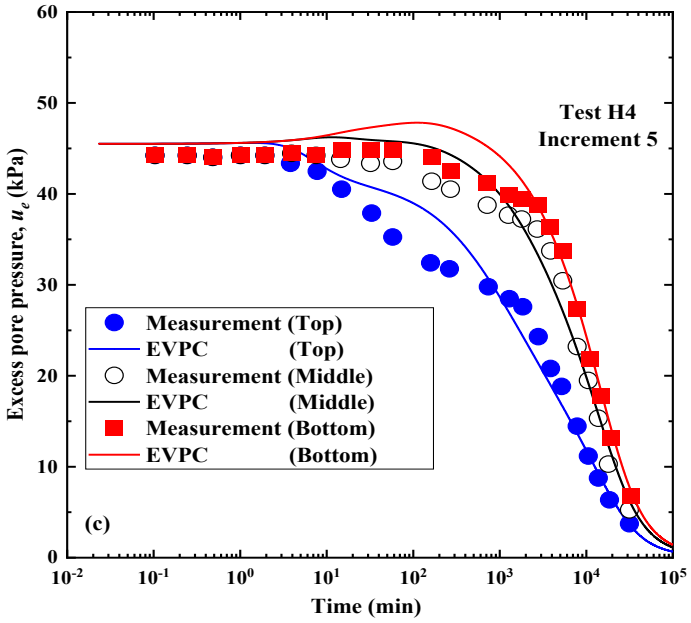

417

418 Fig. 10 Comparison of EVPC simulation and measurements from test H4: (a) average strain vs log t,

419 (b) u_e vs log t for increment 4 and (c) u_e vs log t for increment 5

420 It can be seen from Figs. 8-10 that the EVPC's prediction of the average strain is basically

421 consistent with the measurement results from the oedometer tests. However, the model's prediction

422 of u_e is larger than the measurements observed during the early stage of consolidation testing,

423 especially in the case of increment 4 (meaning that the specimens are over-consolidated). The main

reason for this observation is probably due to the assumption of constant values of C_k, κ and λ. Furthermore, double-S shaped excess pore pressure curves are indicated for both oedometer test and EVPC simulation, especially for increment 4. This effect was systematically investigated by Liu and Borja (2022) and may be attributed to the rate-dependent constitutive response of the soil skeleton. As stated by Liu and Borja (2022), two different settlement stages would be included during the consolidation process. The first and second stages closely related to elastic deformation and viscoplasticity strain, respectively, corresponding to different strain rates and pore pressure dissipation rates.

4 Case study with probabilistic analysis

Probabilistic analysis is conducted with the EVPC to predict settlement and distribution of excess pore water pressures at various time points for the well-instrumented Berthierville site near the St. Lawrence River embankments between Quebec City and Montreal, as reported by Kabbaj et al. (1988). This area is characterised by thick 53-73 m clay deposits lying on bedrock and covered by 10-15 m of recent deposits generated from Lampsilis Lake. The thickness of the topsoil is approximately 0.1-0.2 m. Beneath the topsoil layer is a layer of medium-fine sand, a layer of soft grey silty clay and a layer of fine sand in that order. The thickness of the medium-fine sand layer and the soft grey silty clay are about 2.15 m and 3.2 m, respectively. The relatively homogeneous clay layer between the two sand layers provided excellent conditions for investigating the consolidation behaviour of Berthierville clay layer.

444 The elevation of Berthierville clay layer is between 7.35 m and 4.15 m. The silt content of
445 Berthierville clay is about 62% ~ 68%, and the sand content is negligible. The water content of the
446 clay layer is around 47% ~ 62%, and the plastic limit (w_p) and liquid limit (w_L) are 20% ~ 25% and
447 35% ~ 50%, respectively. Moreover, the Berthierville clay is slightly over-consolidated, with an
448 average over-consolidation ratio of 1.3 ~ 1.4 and an initial void ratio of 1.73 ~ 1.45 based on the
449 measurements of oedometer test by Kabbaj et al. (1988). The mean (μ), autocorrelation length (θ),
450 and coefficient of variation (*COV*) for the three random variables, e_o, w_L and I_p, which are assumed
451 on the basis of test measurements, are summarised in Table 4. For the cross-correlation of random
452 variables, ρ_{e_o,w_L}, ρ_{e_o,I_p} and ρ_{w_L,I_p} are set to 0.2, 0.2 and 0.5, respectively.

453 Table 4. Random variables for consolidation probabilistic analysis of Berthierville clay layer

Parameters	μ (%)	*COV*	θ (m)
e_o	1.6	0.1	1
w_L	62	0.1	1
I_p	34	0.1	1

454

455 The Berthierville clay layer, with H_o = 3.2 m, is divided into 100 elements with the same
456 thickness in the EVPC model. Once the random fields of e_o, w_L and I_p are obtained and the generated
457 random variable values are assigned to the corresponding elements in the model, the corresponding
458 C_c, C_α and k for each element could be determined following the procedures used in previous studies
459 by Jin et al. (2019, 2020):

460 $$C_c = 0.3206ew_L - 0.0284e\left(w_L I_p\right)^2 + 0.0213\left(ew_L I_p\right)^2 - \frac{0.1412\left(w_L\right)^2}{I_p} - 0.0540\left(e\right)^2 w_L I_p + 1.5925 \quad (28)$$

461 $$C_\alpha = \exp\left(0.9092\frac{CI^2}{w_L I_p} + 0.6283\frac{CI^2}{w_L I_p} - 10.3212\left(I_p CI\right)^2 - 0.1963\left(\frac{CI}{w_L I_p}\right)^2 + 3.9741\left(I_p\right)^2 \right) e - 5.1618$$

462 (29)

463 $$\log k = \left(-1.0334 I_p + 0.9435\frac{w_L^2}{I_p} + \frac{0.0762}{w_L I_p} \right) e - 10.219 \quad \left(m/s\right) \tag{30}$$

464 where CI is the clay content of soil (constant CI = 27% is adopted in the simulations), while $\lambda = C_c$
465 /ln10 and $\psi = C_\alpha$ / ln10. Following Terzaghi (1943) and Yin (2015), κ/λ = 1/50 ~ 1/5, and $\kappa = 0.08\lambda$
466 is adopted for this case. In addition, other input initial soil parameters, including σ_o' = 47 kPa, σ_r'
467 = 67 kPa and t_o = 1440 min, are assumed to be constant.

468 The diameters of the crest, height and slope of the test embankment are 24 m, 2.4 m and vertical:
469 horizontal = 1:2, respectively. The conditions of the 3.2 m clay layer under the embankment with
470 such a diameter could be characterised as double-drained one-dimensional consolidation. The
471 construction of test fill was completed in four days, and a gravel layer 10 cm in thickness was placed
472 on top to protect the fill from wind and vegetation. A stress increase of 39 kPa was measured on the
473 ground after the construction of the embankment which then further increased to 44 kPa due to heavy
474 rain three weeks later, as shown in Fig. 11. The change in the load applied to the clay layer is also
475 considered in the EVPC simulations.

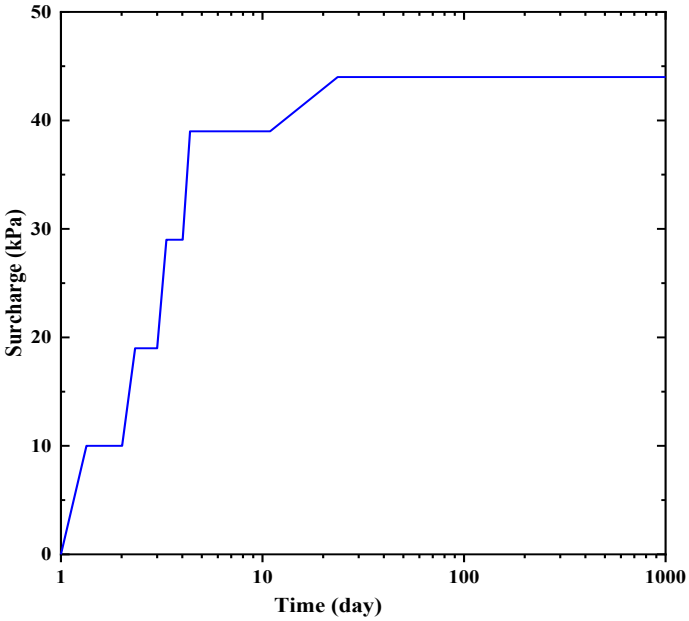

476

477 Fig. 11 Surcharge applied on the clay layer for EVPC simulation (after Kabbaj et al., 1988)

478

479 Fig. 12 compares the settlement results from the EVPC (1000 realisations) and the field
480 measurements presented by Kabbaj et al. (1988). All measured results are within the range of
481 settlement of probabilistic analysis simulations. The settlement is about 0.366 m at t =1002 days
482 (Kabbaj et al., 1988), corresponding to a strain of 11.6%; meanwhile, the probability density
483 distribution of settlement on that day is shown in Fig. 13. The probability of the estimated settlement
484 range of 0.36 m ~ 0.37 m, about 65%, is the largest.

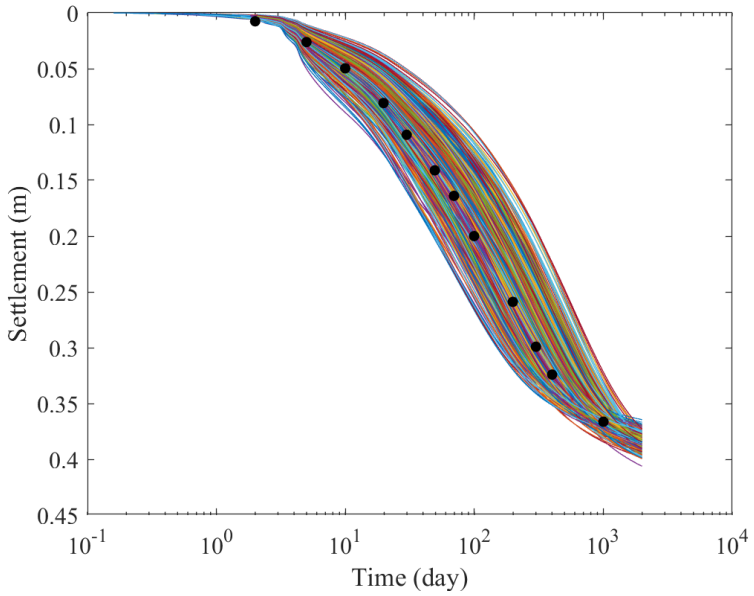

485

486 Fig. 12 Comparison of settlement from probabilistic analysis (1000 realisations) and field

487 measurements (black dot, from Kabbaj et al., 1988)

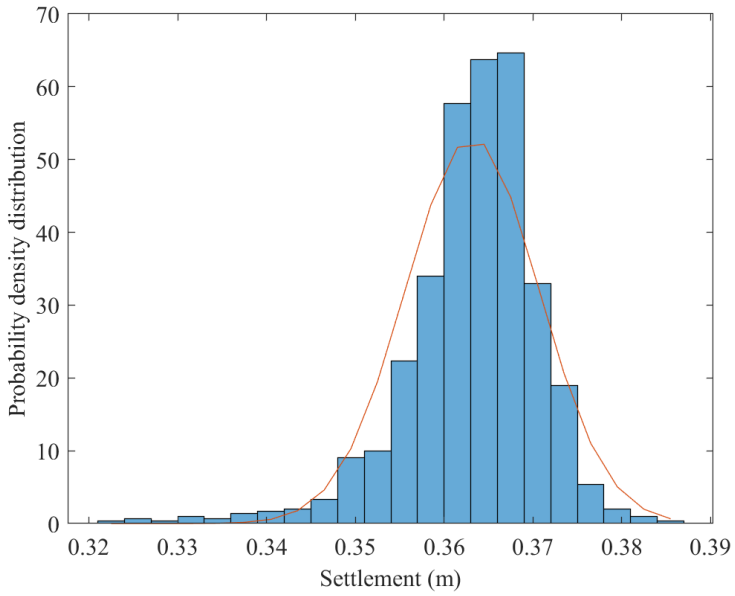

488

489 Fig. 13 Probability density distribution of settlement at 1002nd days

490

491 Fig. 14 compares the measured and simulated (1000 realisations) excess pore water distribution

492 at different times (specifically, 10, 25, 50, 100, 200 and 350 days). Similar to the comparison results

493 of settlement, all of the values of monitored excess pore water pressure fall within the range of the

simulated results. The maximum excess pore water pressures at t = 10, 25, 50, 100, 200 and 350 days are 25.9, 24.8, 23.8, 22.8, 15.9 and 9.6 kPa, respectively. The simulated maximum excess pore water pressure with the highest probability density at t = 100, 200 and 350 days, as shown in Fig.15, is about 23, 15 and 10 kPa, respectively. The dispersion of the maximum excess pore water pressure is larger than that of the settlement, indicating that the excess pore water pressure is more sensitive to the spatial variability of the soil parameters than the settlement. In general, the high probability calculation results of the simulations taking into account the spatial variability of soil compression and hydraulic conductive correlated closely to the field measurements.

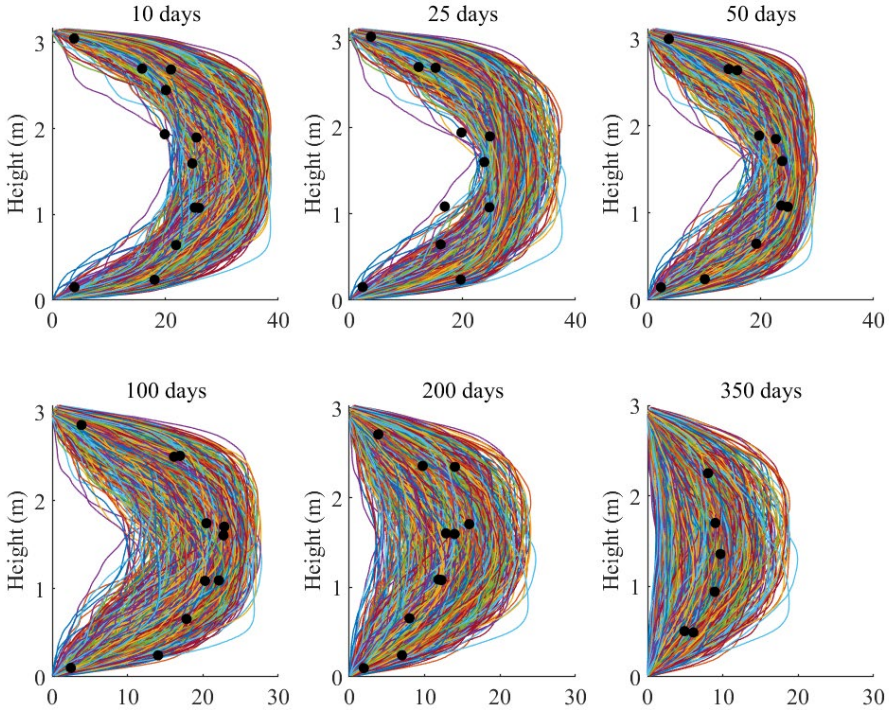

Fig. 14 Comparison of distribution of excess pore water pressure for probabilistic analysis (1000 realisations) and field measurements (black dot, from Kabbaj et al., 1988)

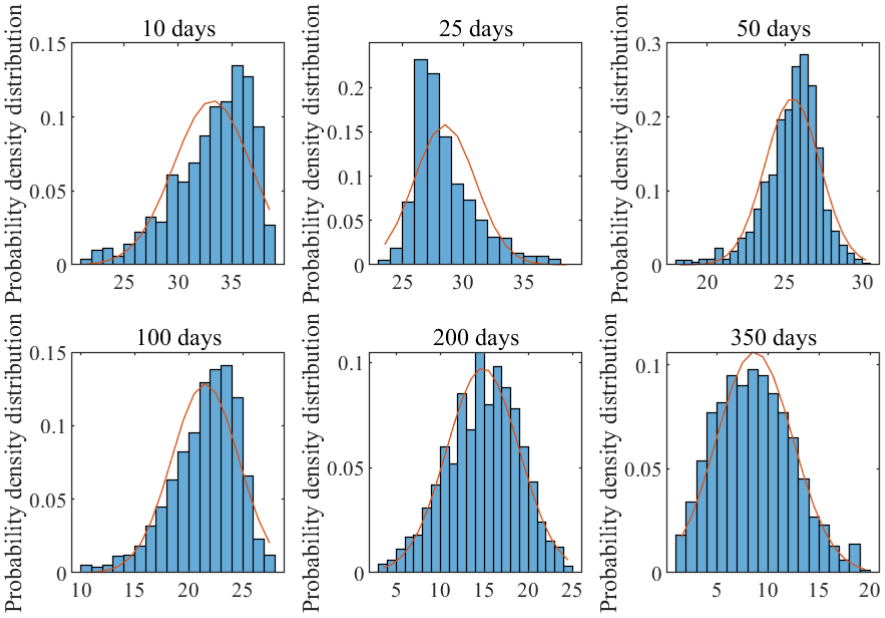

Fig. 15 Probability density distribution of the maximum values of excess pore water pressure at different time points

5 Conclusions

This study presents a 1-D finite strain consolidation model, called EVPC, that combines the piecewise-linear CS2 method and the elastic visco-plastic (EVP) constitutive model, and accounts for the nonlinearity and spatial variability of soil parameters. The following conclusions emerged from the study findings:

(1) The EVPC is a consolidation model that takes into account of finite strain, time-dependent compression relationship (i.e., creep effect), soil self-weight, nonlinear hydraulic conductivity in the consolidation procedure, time-dependent loading, and the spatial variability of hydraulic conductivity and compressibility. Model development included the adoption of an elastic visco-plastic constitutive relationship based on the concept of ‘equivalent time’. In addition, the

519 EVPC includes the assumption that creep strain happens in the entire consolidation procedure;
520 that is, hypothesis B is valid.
521 (2) The accuracy of the EVPC deterministic analysis is compared with the finite element solutions
522 (i.e., PLAXIS with soft soil creep model) through idealised problems involving different initial
523 layer heights, instantaneous load and step loads. Good agreement is observed for the EVPC
524 simulations and PLAXIS results, including settlement and excess pore water pressure.
525 Afterwards, the EVPC results are further compared with oedometer test data for specimens of
526 different thicknesses. The soil parameters used for simulations are derived from one of the
527 oedometer test measurements and then adopted to estimate the consolidation behaviour of other
528 thicker specimens. Overall agreement is observed for the strain results yielded by the EVPC and
529 oedometer test measurements. Substantial differences are observed from the measured and
530 estimated excess pore water pressure results during the early stage of consolidation, especially
531 for increment 4, probably because the constant parameters κ, λ and C_k could not describe the
532 compression and permeability constitutive over such a wide range.
533 (3) EVPC probabilistic analysis is adopted to estimate the consolidation behaviour of Berthierville
534 clay under the embankment construction site near the St Laurent River, Canada. The field
535 measurements of settlement and excess pore water pressure distribution fell within the high
536 probability density results of the simulations. The discreteness of the simulation results for excess
537 pore water pressure is larger than that for settlement, indicating that excess pore water pressure is
538 more sensitive to the spatial variability of soil parameters (specifically, hydraulic conductivity
539 and compressibility).

Acknowledgments

This research was supported by the Research Impact Fund of Research Grants Council (RGC) of Hong Kong Special Administrative Region Government (HKSARG) of China (Grant No.: R5037-18F). This financial support is gratefully acknowledged.

References

Alibeikloo, M., Khabbaz, H., and Fatahi, B. 2022. Random field reliability analysis for time-dependent behaviour of soft soils considering spatial variability of elastic visco-plastic parameters. Reliability Engineering & System Safety, 219, 108254.

Berre, T., and Iversen, K. 1972. Oedometer tests with different specimen heights on a clay exhibiting large secondary compression. Géotechnique, 22(1), 53-70.

Bjerrum, L. 1967. Engineering geology of Norwegian normally-consolidated marine clays as related to settlements of buildings. Géotechnique, 17(2), 83-118.

Borja, R. I., and Alarcón, E. 1995. A mathematical framework for finite strain elastoplastic consolidation Part 1: Balance laws, variational formulation, and linearization. Computer Methods in Applied Mechanics and Engineering, 122(1-2), 145-171.

Borja, R. I., Tamagnini, C., and Alarcón, E. 1998. Elastoplastic consolidation at finite strain part 2: finite element implementation and numerical examples. Computer Methods in Applied Mechanics and Engineering, 159(1-2), 103-122.

Carter, J. P., Booker, J. R., and Small, J. C. 1979. The analysis of finite elasto-plastic consolidation. International Journal for Numerical and Analytical Methods in Geomechanics, 3(2), 107-129.

Feldkamp, J. R. 1989. Numerical analysis of one-dimensional nonlinear large-strain consolidation by the finite element method. Transport in porous media, 4(3), 239-257.

Fox, P. J., and Berles, J.D., 1997. CS2: a piecewise-linear model for large strain consolidation. International Journal for Numerical and Analytical Methods in Geomechanics, 21(7), 453-475.

566 Fox, P. J., Di Nicola, M., and Quigley, D.W. 2003. Piecewise-linear model for large strain radial
567 consolidation. Journal of Geotechnical and Geoenvironmental Engineering, 129(10), 940-950.
568 Fox, P. J., Pu, H. F., and Berles, J. D. 2014. CS3: Large strain consolidation model for layered soils.
569 Journal of Geotechnical and Geoenvironmental Engineering, 140(8), 040414041.
570 Garlanger, J. E. 1972. The consolidation of soils exhibiting creep under constant effective stress.
571 Géotechnique, 22(1), 71-78.
572 Gibson, R. E., England, G.L., and Hussey, M.J.L. 1967. The theory of one-dimensional consolidation
573 of saturated clays: I. finite non-linear consolidation of thin homogeneous layers. Géotechnique,
574 17(3), 261-273.
575 Griffiths, D. V., and Fenton, G. A. 2004. Probabilistic slope stability analysis by finite elements.
576 Journal of Geotechnical and Geoenvironmental Engineering, 130(5), 507-518.
577 Hu, Y. Y., Zhou, W. H., and Cai, Y. Q. 2014. Large-strain elastic viscoplastic consolidation analysis
578 of very soft clay layers with vertical drains under preloading. Canadian Geotechnical Journal,
579 51(2), 144-157.
580 Huang, J., Griffiths, D. V., and Fenton, G. A. 2010. Probabilistic analysis of coupled soil
581 consolidation. Journal of Geotechnical and Geoenvironmental Engineering, 136(3), 417-430.
582 Jin, Y. F., and Yin, Z. Y. 2020. An intelligent multi-objective EPR technique with multi-step model
583 selection for correlations of soil properties. Acta Geotechnica, 15(8), 2053-2073.
584 Jin, Y. F., Yin, Z. Y., Zhou, W. H., Yin, J. H., and Shao, J. F. 2019. A single-objective EPR based
585 model for creep index of soft clays considering L2 regularization. Engineering Geology, 248,
586 242-255.
587 Kabbaj, M., Tavenas, F., and Leroueil, S. 1988. In situ and laboratory stress-strain relationship.
588 Géotechnique, 38(1), 83-100.
589 Kutter, B. L., and Sathialingam, N. 1992. Elastic-viscoplastic modelling of the rate-dependent
590 behaviour of clays. Géotechnique, 42(3), 427–441.
591 Lee, K., and Sills, G.C. 1981. The consolidation of a soil stratum, including self-weight effects and
592 large strains. International Journal for Numerical and Analytical Methods in Geomechanics, 5,
593 405-428.

Leroueil, S., Kabbaj, M., Tavenas, F., and Bouchard, R. 1985. Stress-strain-stress rate relation for the compressibility of sensitive natural clays. Géotechnique, 35(2), 159-180.

Li, P. L., Yin, J. H., Yin, Z. Y., and Chen, Z. J. 2023. One-dimensional nonlinear finite strain analysis of self-weight consolidation of soft clay considering creep. Computers and Geotechnics, 153, 105081.

Liu, Y., and Borja, R. I. 2022. Time scales in the primary and secondary compression of soils. International Journal for Numerical and Analytical Methods in Geomechanics, 46(8), 1383-1408.

McNabb, A. 1960. A mathematical treatment of one-dimensional soil consolidation. Quarterly of Applied Mathematics, 17, 337-347.

McVay, M. C., Townsend, F. C., and Bloomquist, D.G. 1989. One-dimensional Lagrangian consolidation. Journal of Geotechnical Engineering, 115(6), 893-898.

Nazem, M., Sheng, D., Carter, J. P., and Sloan, S. W. 2008. Arbitrary Lagrangian-Eulerian method for large‐strain consolidation problems. International Journal for Numerical and Analytical Methods in Geomechanics, 32(9), 1023-1050.

Nguyen, B. P., Do, T. H., and Kim, Y. T. 2020. Large-strain analysis of vertical drain-improved soft deposit consolidation considering smear zone, well resistance, and creep effects. Computers and Geotechnics, 123, 103602.

Salgado, R., and Kim, D. 2014. Reliability analysis of load and resistance factor design of slopes. Journal of Geotechnical and Geoenvironmental Engineering, 140(1), 57-73.

Song, D. B., Pu, H. F., Khoteja, D., Li, Z. Y., and Yang, P. 2021. One-dimensional large-strain for soft soil consolidation induced by vacuum-assisted prefabricated horizontal drain. European Journal of Environmental and Civil Engineering, 26(11), 5496-5516.

Terzaghi, K. 1943. Theoretical soil mechanics. New York, John Wiley.

Vermeer, P. A., and Neher, H. P. 1999. A soft soil model that accounts for creep. In Beyond 2000 in computational geotechnics: 10 years of PLAXIS international, pp. 249-262. Rotterdam, the Netherlands: Balkema.

Xie, K. H., and Leo, C.J. 2004. Analytical solutions of one-dimensional large strain consolidation of saturated and homogeneous clays. Computers and Geotechnics, 31(4), 301-314.

622 Xu, B. H., Indraratna, B., Rujikiatkamjorn, C., and Nguyen, T. T. 2022. A large-strain radial
623 consolidation model incorporating soil destructuration and isotache concept. Computers and
624 Geotechnics, 147, 104761.
625 Yang, J., Yin, Z. Y., Laouafa, F., and Hicher, P. Y. 2019. Analysis of suffusion in cohesionless soils
626 with randomly distributed porosity and fines content. Computers and Geotechnics, 111, 157-171.
627 Yin, J. H. 2015. Fundamental issues of elastic viscoplastic modeling of the time-dependent stress–
628 strain behavior of geomaterials. International Journal of Geomechanics, 15(5), A4015002.
629 Yin, J. H. and Graham, J. 1994. Equivalent times and one-dimensional elastic viscoplastic modelling
630 of time-dependent stress-strain behaviour of clays. Canadian Geotechnical Journal, 31(1), 42-52.
631 Yin, J. H. and Graham, J. 1996. Elastic visco-plastic modelling of one-dimensional consolidation.
632 Géotechnique, 46(3), 515-527.
633 Yin, J. H., and Feng, W. Q. 2017. A new simplified method and its verification for calculation of
634 consolidation settlement of a clayey soil with creep. Canadian Geotechnical Journal, 54(3),
635 333-347.
636 Yin, J. H., and Graham, J. 1989. Viscous-elastic-plastic modelling of one-dimensional
637 time-dependent behaviour of clays. Canadian Geotechnical Journal, 26(2), 199-209.
638 Yin, J., Graham, J., Clark, J. I., and Gao, L. 1994. Modelling unanticipated pore-water pressures in
639 soft clays. Canadian Geotechnical Journal, 31(5), 773-778.
640 Yin, Z. Y., Chang, C. S., Karstunen, M., and Hicher, P. V. 2010. An anisotropic elastic-viscoplastic
641 model for soft clays. International Journal of Solids and Structures, 47(5), 665-677.
642 Yin, Z. Y., Karstunen, M., Chang, C. S., Koskinen, M., and Lojander, M. 2011. Modeling
643 time-dependent behavior of soft sensitive clay. Journal of Geotechnical and Geoenvironmental
644 Engineering, 137(11): 1103-1113.
645 Zhang, Q., Chen, Y., Yang, Z., and Darve, E., 2020. Multi-constitutive neural network for large
646 deformation poromechanics problem. Presented at the Proceedings of the Machine Learning and
647 the Physical Sciences Workshop, 34th Conference on Neural Information Processing Systems
648 (NeurIPS), Virtual (Online).

649 Zhao, Y., and Borja, R. I. 2020. A continuum framework for coupled solid deformation–fluid flow
650 through anisotropic elastoplastic porous media. Computer Methods in Applied Mechanics and
651 Engineering, 369, 113225.
652
653

654 ## Notation

C_c compression index

C_α secondary compression index

CI clay content of soil

e void ratio

G_s specific gravity of solids

h total water head

H_o initial height of soil layer

H height of soil layer

i hydraulic gradient

I_p plasticity index

j coordinate of element

k coefficient of permeability

k_s equivalent coefficient of permeability

L_o initial thickness of element

L thickness of element

N_f number of Monte Carlo simulations

R_j number of elements

S settlement

t time

t_e equivalent time

t_o parameter for choice of reference time line

u pore water pressure

u_e excess pore water pressure

V specific volume

v_{rf} discharge velocity of fluid relative to solid phase

w_p plastic limit

z vertical coordinate

Δq change in the overburden stress

Δt time increment

γ saturated unit weight

γ_w unit weight of pore water

σ total stress

σ' effective stress

$\sigma_o^{'}$ initial effective stress

$\sigma_i^{'}$ unit effective stress

$\sigma_{ro}^{'}$ parameter similar to pre-consolidation pressure

ε_i^e strain at $\sigma' = \sigma_i^{'}$

ε_o^r strain at $\sigma' = \sigma_{ro}^{'}$

κ logarithmic material constant for instantaneous strains

λ logarithmic material constant for stress-dependent plastic strains

ψ logarithmic material constant for creep

μ mean

σ standard deviation

ρ correlation coefficient

θ autocorrelation length

ε^e instantaneous strain

ε^r stress-dependent plastic strain

ε^{tp} creep strain

Superscripts

t time

Subscripts

j jth element